Chemical Science

Accepted Manuscript

This article can be cited before page numbers have been issued, to do this please use: M. Kang, Z. Sun, K. Schmidt-Rohr and S. M. Cohen, *Chem. Sci.*, 2026, DOI: 10.1039/D6SC02045C.

ROYAL SOCIETY OF CHEMISTRY

rsc.li/chemical-science

View Article Online
DOI: 10.1039/D6SC02045C

ARTICLE

Quantification of mesopore infiltration in a polymer-grafted metal-organic framework

Received 00th January 20xx,
Accepted 00th January 20xx

DOI: 10.1039/x0xx00000x

Minjung Kang,[a,†] Zhenhuan Sun,[b] Klaus Schmidt-Rohr*[b] and Seth M. Cohen*[a]

Polymer-grafted metal-organic frameworks (MOFs) address the powder form and poor processability of crystalline MOFs by forming free-standing self-assembled MOF monolayers (SAMMs). However, to date, SAMMs have been limited to microporous MOFs. Herein, we report the first successful synthesis of polymer-grafted mesoporous PCN-222 nanorods using chain transfer agents (CTA)-anchored reversible addition-fragmentation chain transfer polymerization (RAFT) polymerization of methyl acrylate (MA) and methyl methacrylate (MMA), extending SAMMs beyond microporous frameworks. Monodisperse PCN-222 nanorods were surface-functionalized and polymer grafts were grown from the particles using optimized photocatalyst conditions. PMMA grafting yields free-standing SAMMs with tunable 1D-2D rod alignments through thick external brushes and partial mesopore infiltration, while flexible PMA causes aggregation and SAMMs failure due to thin surface coverage. Quantitative ^{13}C solid-state nuclear magnetic resonance (ssNMR) reveals polymer-MOF ratios consistent with PMMA's dual surface/partial pore filling (perturbed linker peaks and relaxation), while ^{1}H-^{13}C HetCor with spin diffusion shows rapid initial cross-peaks from proximal polymer. Simulations confirm thicker PMMA brushes (~2x PMA thickness) and significant pore filling, explaining assembly differences when compared to SAMMs derived from other MOFs (e.g., UiO-66). This work establishes polymer rigidity-mesopore interplay as a design principle for high-porosity MOF hybrids, providing a foundation for future development of functional, free-standing SAMMs for catalysis, separation and large-molecule transport applications.

Introduction

Metal-organic frameworks (MOFs) are crystalline porous materials formed by the coordination of metal ions or clusters with multitopic organic linkers. Their precise structural control and high porosity have garnered significant attention over the past few decades.[1-3] The reticular synthesis concept, which systematizes MOF formation principles, enables the design of metal-oxygen cluster-based secondary building units (SBUs) and linkers to construct predictable three-dimensional networks, thereby allowing precise tuning of pore size, chemical environment, and functionality.[4] Building on these design principles, MOFs with diverse pore architectures and surface chemistries have been developed and have demonstrated their potential across a wide range of applications, including gas storage, chemical separation, sensing, and drug delivery.[5-7] Recent efforts have focused on leveraging the high porosity of MOFs with polymers to enhance mechanical strength, processability, and environmental stability.[8, 9] In particular, MOF-polymer hybrid materials combine the rigid crystalline skeletons of MOFs with the flexibility and processability of polymers, emerging as a new class of materials that achieve morphological diversity and functional integration unattainable with conventional porous materials.[5, 9]

Recent studies have focused on direct grafting of polymer chains onto MOF surfaces to modulate interparticle interactions, thereby enabling the formation of novel structures. This approach combines the crystalline framework of MOFs with polymer flexibility, imparting both processability and functional tunability unattainable with conventional inorganic porous materials. Notably, a method utilizing catechol-functionalized chain transfer agents (cat-CTA) to anchor RAFT initiation sites on MOF surfaces, followed by surface-initiated controlled radical polymerization, has been developed, establishing a new synthetic paradigm for polymer-grafted MOFs.[10] Polymer-grafted MOF nanoparticles synthesized by this approach have been shown to self-assemble at the air-water interface into free-standing self-assembled MOF monolayers (SAMMs) with thicknesses in the hundreds of nanometers. These SAMMs maintain high MOF content (>80 wt%) while polymer brushes enhance interparticle cohesion, enabling the formation of stable monolayer films.[11] Subsequent investigations have quantitatively elucidated SAMMs formation mechanisms and systematically analysed the effects of polymer chain length and grafting density on particle alignment and film mechanical properties.[12] The results demonstrate that sufficient surface polymer brushes facilitate uniform, continuous monolayer films through interparticle polymer-polymer entanglement, with chain length exerting a greater

[a] Department of Chemistry and Biochemistry, University of California, San Diego, La Jolla, California 92093, United States. E-mail: scohen@ucsd.edu
[b] Department of Chemistry, Brandeis University, Waltham, Massachusetts 02453, United States.
† Present address: Department of Chemistry Education, Korea National University of Education, Cheongju, Republic of Korea, 28173
Supplementary Information available. See DOI: 10.1039/x0xx00000x

influence on mechanical properties than grafting density. Recent work has further demonstrated that photosensitivity, mechanical strength, or electrical responsiveness can be imparted by tailoring polymer types or functional groups. For instance, photoswitchable SAMMs with light-tuneable ion transport properties have been achieved through grafting of azobenzene-containing copolymers.[13] Thus, research on polymer-grafted MOF-based SAMMs has evolved beyond simple MOF-polymer composites into a versatile platform technology for organizing MOF particles into aligned 2D architectures and transforming them into functional films.

All reported SAMMs studies to date have employed microporous MOFs, particularly the UiO-66(Zr) series, which offer high crystallinity and chemical stability along with uniform polymer chain growth enabled by surface-anchored cat-CTA.[11, 12] To expand the scope of SAMMs, polymer-grafted systems beyond UiO-66 should be explored. While UiO-66 features micropores of 0.8 and 1.1 nm,[14] Zr-TCPP-based mesoporous PCN-222 (TCPP = tetrakis(4-carboxyphenyl) porphyrin; PCN = porous coordination network, Fig. 1) possesses significantly larger channels (~3.7 nm), conferring superior capabilities for accommodating large molecules and enhanced mass transport.[15] PCN-222 demonstrates high-capacity adsorption of large dyes and proteins[16] and leverages porphyrin units for strong visible-light absorption in photocatalysis.[17] Furthermore, integration of these attributes enables efficient catalysis of bulky substrates (e.g., dyes or biomimetic substrates used in peroxidase-mimic reactions) through rapid diffusion and porphyrin-mediated visible-light photocatalysis.[15, 18] Converting versatile PCN-222 into films using SAMM strategies would enhance processability and thereby broaden their applications. However, the influence of MOF pore size on SAMMs systems remains unexplored.

While microporous structures like UiO-66 feature severely restricted pores, mesoporous MOFs such as PCN-222 raise questions regarding whether polymer chains can form proper surface brushes due to mesopore accessibility. Specifically, whether polymer chains remain as surface brushes or infiltrate the MOF pores requires investigation. Additionally, the anisotropic rod-shaped morphology of PCN-222, distinct from the more isotropic UiO-66, necessitates evaluation of uniform polymer grafting across all facets and subsequent SAMMs formation.

Herein, the influence of polymer structural properties and MOF pore architecture on self-assembly behavior is investigated by grafting poly(methyl acrylate) (PMA) and poly(methyl methacrylate) (PMMA) onto the surface of mesoporous PCN-222. Through this approach, research on SAMMs is extended to the mesoporous regime, while elucidating new structural mechanisms governing polymer–MOF interactions. Particular attention is given to the potential for concurrent polymer chain infiltration into mesoporous PCN-222 channels and surface brush formation, with experimental analysis of how polymer type and pore structure interplay to determine SAMMs formation and film properties using solid-state nuclear magnetic resonance (ssNMR) spectroscopy with ^{1}H spin diffusion[19] to probe chain infiltration into the pores. As the first demonstration of mesoporous MOF-based SAMMs, this work provides new directions for structural design of high-porosity MOF-polymer hybrids and development of functional free-standing films.

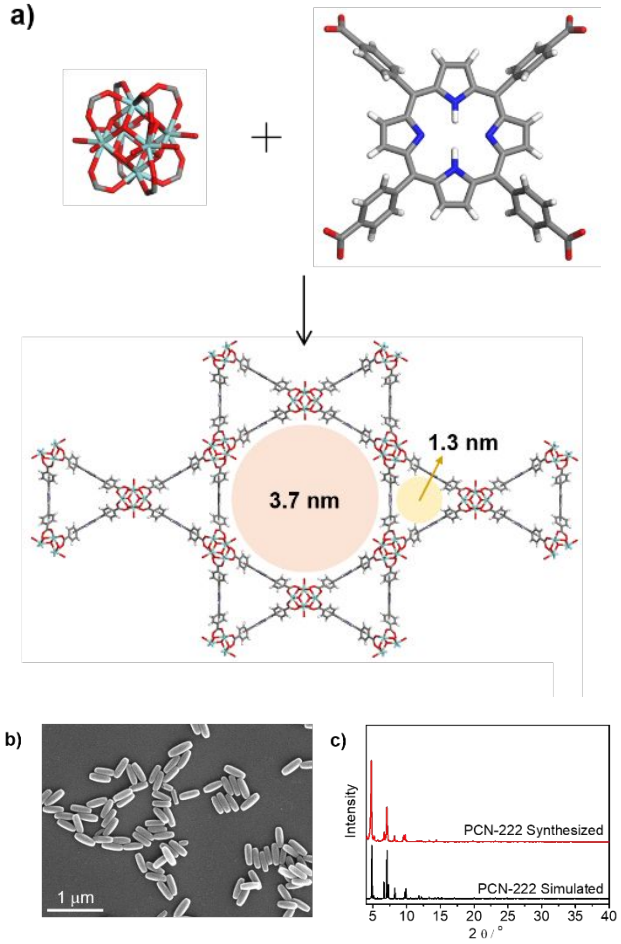

Fig. 1 Characterization of rod-shaped PCN-222 nanorods. (a) Building blocks of PCN-222 and structural model showing 3.7 nm mesopore channels. (b) SEM image (scale bar: 1 μm). (c) PXRD pattern matching simulated data.

Results and Discussion

Synthesis of PCN-222 nanorods and surface-grafted polymers.

PCN-222 is a representative mesoporous MOF constructed from $Zr_6(\mu_3\text{-}O)_8(OH)_8$ clusters and TCPP linkers. It features one-dimensional channels with a diameter of ~3.7 nm, auxiliary micropores of about 1.3 nm, and exhibits high chemical stability and crystallinity (Fig. 1a).[15] In this study, PCN-222 particles with uniform size were synthesized under solvothermal conditions by combining $ZrOCl_2{\cdot}8H_2O$ with TCPP while preserving these structural characteristics. In particular, difluoroacetic acid (DFA) was employed as a modulator to control the particle growth rate, enabling the successful preparation of monodisperse rod-shaped PCN-222 with an average length of ~380 nm (Fig. 1b).[19] DFA provides more precise control compared to more conventional modulators (e.g., benzoic acid or acetic acid) and promotes more uniform nucleation and slower crystal growth, ultimately leading to highly

View Article Online
DOI: 10.1039/D6SC02045C

monodisperse PCN-222 particles. SEM analysis of the synthesized PCN-222 samples clearly revealed a uniform rod-shaped morphology (Fig. 1b), with particle lengths and diameters of approximately 380±20 nm and 140±10 nm, respectively, in good agreement with reported values.[19] To evaluate the crystallinity, powder X-ray diffraction (PXRD) patterns were collected for the deep purple PCN-222 powders (Fig. 1c). The experimental patterns matched well with the simulated pattern from the reported single-crystal structure, demonstrating that the synthesized material is phase-pure PCN-222 with the expected framework structure. The distinctive reflections observed in the low 2θ region indicate a high degree of mesopore ordering and, as shown in Fig. 1a, PCN-222 features large one-dimensional mesopore channels with diameters of up to about 3.7 nm.

To graft polymers onto the surface of PCN-222, previously synthesis protocols were adapted from reported UiO-66-based SAMMs (Scheme 1).[11, 12, 20] First, CTAs bearing catechol groups were synthesized and immobilized on the PCN-222 surface through catechol-Zr(IV) coordination. The synthesis of each CTA and the introduction of the catechol functionality were carried out following reported procedures with minor modifications (Scheme S1-S4).[11, 12] In designing these CTAs, the combination of monomer and CTA radical stability required for the subsequent polymerization step was taken into account[21]: 2-(dodecylthiocarbonothioylthio)-2-methylpropionic acid (DDMAT) was employed as the CTA for methyl acrylate (MA) polymerization, whereas 4-cyano-4-[(dodecylsulfanylthiocarbonyl)sulfanyl]pentanoic acid (CDSPA) was used as the CTA for methyl methacrylate (MMA) polymerization. The catechol-functionalized DDMAT and CDSPA derivatives were prepared via activated-ester coupling with dopamine and then grafted to the MOF using a biphasic chloroform-water procedure analogous to that reported for UiO-66 (Scheme S5). Through this procedure, PCN-222-DDMAT and PCN-222-CDSPA samples were obtained, in which RAFT initiating sites are immobilized on the MOF surface.

Subsequently, surface-initiated photoinduced electron transfer-RAFT polymerization (SI-PET-RAFT) was employed to grow polymer chains from the PCN-222 surface. The reactions were carried out in dimethyl sulfoxide (DMSO) using purified MA or MMA monomers, with tris(2-phenylpyridine)iridium ($Ir(ppy)_3$) as the photocatalyst and a blue light-emitting diode (LED) light source (λ= 455 nm). These reaction conditions were previously shown to afford excellent control in UiO-66-based systems (Scheme S6-S7).[11, 12, 20] In all polymerizations, a certain amount of free CTA (without the catechol anchor) was added to the reaction mixture along with the surface-bound catechol-CTA in order to maintain efficient RAFT control even when the exact surface CTA loading was unknown, following established SI-PET-RAFT protocols.[11] In contrast to the colourless UiO-66 particles, which allow relatively uniform penetration of blue light throughout the reaction medium, the PCN-222 particles exhibit a deep purple colour due to the strong absorption of the porphyrin ligands, severely limiting light penetration into the bulk of the suspension. Under otherwise identical photoinitiation conditions, ^{1}H NMR analysis of the reaction mixture showed a significantly reduced monomer-to-polymer conversion, as quantified from the integrals of the monomer methyl resonances and the corresponding polymer signals, indicating insufficient activation in the interior of the reaction volume. To compensate for this limited light penetration, the photocatalyst concentration was increased relative to the original protocol, which enabled a high degree of conversion after 8 h of LED irradiation. In the case of MA polymerization, the photocatalyst loading was increased tenfold, whereas for MMA, it was doubled. These conditions were identified through an optimization process aimed at obtaining samples with comparable polymer contents. After polymerization, the PCN-222-PMA and PCN-222-PMMA particles were purified by repeated cycles of centrifugation, decanting, and redispersion in acetone followed by toluene, analogous to the work-up procedures reported for UiO-66-based systems, and the resulting samples were used for SAMMs formation experiments. The detailed synthetic procedures are provided in the Supporting Information.

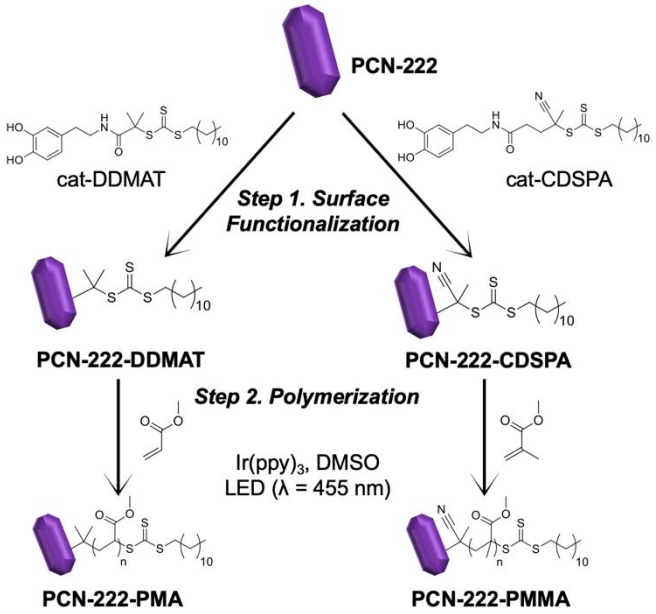

Scheme 1. Synthetic strategy for polymer-grafted PCN-222 via catechol-CTA immobilization and SI-PET-RAFT polymerization of MA or MMA.

Thermogravimetric analysis (TGA) was employed to quantify the polymer fraction in the resulting PCN-222-PMA and PCN-222-PMMA samples. Taking advantage of the distinct thermal stabilities and decomposition temperatures of the MOF and polymer components, the polymer weight fraction within each hybrid material was determined, revealing values of 40.1 wt% for PCN-222-PMA and 46.9 wt% for PCN-222-PMMA (Figs. S1, S2 and Table S1). These results indicate that, after multiple washing steps to remove free polymer from the suspension, the remaining solids still contained a substantial polymer fraction originating exclusively from chains grafted to the MOF surface, consistent with the successful formation of polymer-grafted PCN-222. To analyse the molecular characteristics of the grafted polymers, the MOF was digested with hydrofluoric acid

(HF) to isolate the polymer, followed by gel permeation chromatography (GPC) for molecular weight analysis; however, the resulting data were difficult to interpret unambiguously (Table S1, Fig. S3). In this system, polymer brushes grown on the anisotropic PCN-222 surface exhibited bimodal peaks and anomalously high apparent molecular weights in GPC. These features can be attributed to multiple factors: position-dependent surface curvature and local initiator density across the MOF particles, intermolecular chain transfer (so-called 'backbiting') within surface-grafted acrylate chains, which generates covalently bound short-chain segments,[22-24] and the elevated photocatalysis loadings employed to compensate for the strong light absorption of PCN-222. This behaviour is consistent with recent reports on spherical nanoparticles, where variations in surface curvature, initiator density, and catalyst concentration lead to heterogeneous molecular weight distributions and initiation efficiencies in surface-grafted brushes,[22] and in the present PCN-222 system the combined effects of complex surface topology and curvature distribution clearly impacted the polymer characteristics.

Self-assembly of polymer-grafted PCN-222 into SAMMs.

The self-assembly behaviour of the synthesized polymer-grafted PCN-222 samples was investigated by attempting SAMMs formation at an air-water interface using toluene as the dispersing solvent (Scheme S10). A small droplet of a toluene suspension of PCN-222-PMA or PCN-222-PMMA was gently deposited onto the water surface in a Petri dish, where it rapidly spread to cover the interface; the dish was then covered to minimize disturbance while the toluene slowly evaporated, allowing the particles to assemble at the interface. Fig. 2 presents SEM images comparing the resulting interfacial assemblies obtained from PCN-222-PMA and PCN-222-PMMA. For PCN-222-PMMA, SAMMs formation was successful. As the toluene evaporated, a thin, brittle film characteristic of PMMA-grafted MOF assemblies formed on the water surface, and wrinkles were observed that originated at the outer edge where toluene dried first and then drying propagated toward the centre as the film contracted (Fig. 2a). These wrinkles are consistent with differential drying and contraction and serve as evidence for continuous film formation. The resulting film could be lifted using a Cu wire loop in a mechanical lifting test, confirming that it could be maintained as a free-standing membrane. SEM analysis revealed a well-aligned monolayer of rod-shaped MOFs (Fig. 2b). Furthermore, a range of ordered architectures were observed as a function of particle density: individually dispersed particles at very low surface coverage, one-dimensional ribbon-like arrangements at low surface coverage, two-dimensional monolayer films at intermediate coverage, and multilayer structures at high coverage. The SEM images corresponding to each stage are shown in Fig. S4. This structural diversity indicates that interparticle interactions mediated by the surface polymer brush can be tuned to control particle packing, highlighting the potential for structural design via particle arrangement. Additionally, the distinct crystallographic facets of PCN-222 nanorod – hexagonal end facets and lateral side facets with differing surface Zr(IV) node densities – are expected to result in facet-dependent grafting density differences, which may further contribute to the observed anisotropic interparticle interactions. Taken together, these observations demonstrated that, despite the mesoporous nature of PCN-222, PMMA brushes on the MOF surface enable effective polymer-polymer interactions between particles, allowing the formation of free-standing SAMMs.

In contrast, PCN-222-pMA did not form SAMMs. When a toluene suspension of PCN-222-PMA was deposited onto the water surface, macroscopic particle aggregation was observed during solvent evaporation, indicating that the particles failed to distribute uniformly at the air-water interface and instead clustered locally (Fig. 2c). Notably, such pronounced aggregation behaviour was not observed for PMA-grafted samples based on other MOFs, which remained well-dispersed in toluene and readily formed SAMMs under identical assembly conditions.[11, 12] SEM images likewise revealed irregular agglomerates rather than a continuous layer-like arrangement, even though voids remained between particles (Fig. 2d). Furthermore, during solvent exchange into toluene after polymer grafting, PCN-222-PMA exhibited markedly poorer dispersibility and more readily formed aggregates compared to the other polymer-grafted samples (Fig. S5). This behaviour suggests that the particle surface is not sufficiently hydrophobic for toluene to act as a good solvent, implying that a well-developed surface polymer brush is not established. As a consequence, PMA-grafted PCN-222 is unable to generate adequate polymer-polymer interactions between particles, and self-assembly into SAMMs fails.

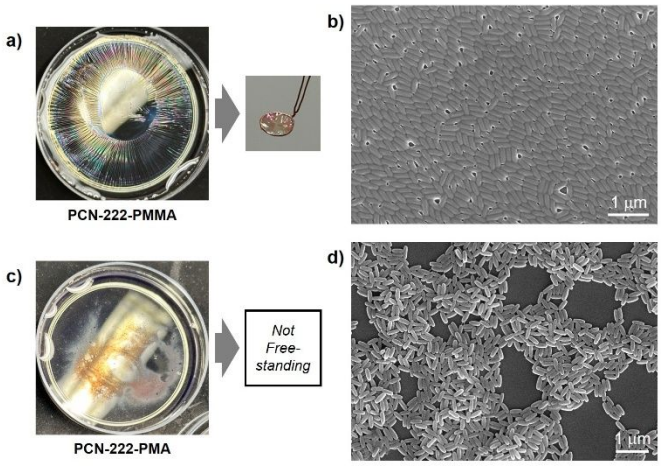

Fig. 2 Interfacial self-assembly of polymer-grafted PCN-222 at an air-water interface. (a) Macroscopic wrinkles film formed by PCN-222-PMMA during toluene evaporation. (b) SEM image of aligned PCN-222-PMMA monolayer (scale bar: 1 μm). (c) Macroscopic aggregation of PCN-222-PMA particles. (d) SEM image of irregular PCN-222-PMA agglomerates (scale bar: 1 μm).

To gain structural insight into the contrasting SAMMs-forming characteristics of PCN-222-PMA and PCN-222-PMMA, solid-state nuclear magnetic resonance (ssNMR) spectroscopy

was employed. The analysis included not only the PCN-222-based samples but also previously reported UiO-66-PMA and UiO-66-PMMA, which were synthesized with minor modifications to the methods previously reported in the literature (Scheme S8-S9).[11, 12] UiO-66 possesses a microporous structure with pore sizes of 0.8 and 1.1 nm. PMA forms relatively flexible chains with a lower glass transition temperature ($T_g \approx 8$ °C),[25] whereas PMMA exhibits a higher glass transition temperature ($T_g \approx 105$ °C)[26] and correspondingly more rigid chains. Accordingly, in a tight micropore environment such as UiO-66, it is reasonable to expect that the more flexible PMA chains can partially infiltrate the internal pores, whereas the bulkier and more rigid PMMA chains are effectively excluded. By contrast, the large mesoporous channels of PCN-222 should be sufficiently wide to permit not only partial penetration by flexible PMA chains, but potentially also some degree of infiltration by the more rigid PMMA chains. These considerations serve as a working hypothesis to rationalize the role of pore size and polymer rigidity, which is then examined more quantitatively by ssNMR analysis.

NMR composition analysis.

Fig. 3 compares solid-state ^{13}C NMR spectra of polymer-grafted and neat PCN-222. PCN-222-PMMA(high), which has a higher polymer content than PCN-222-PMMA, serves as a reference in Fig. 3a. It was synthesized using the same protocol as PCN-222-PMMA but with a tenfold increased $Ir(ppy)_3$ photoinitiator loading (0.015 equiv.) compared to the original UiO-66-based synthesis. This condition, initially explored during synthesis optimization, yielded a high polymer fraction of 68.5% by TGA. The integrated intensity of the PMA bands is less than half of the area of the PMMA signals in Fig. 3a, which indicates a significantly smaller PMA:MOF than PMMA:MOF ratio, while the match is much better with a composite with lower PMMA fraction in Fig. 3b. Quantitative direct-polarization ^{13}C NMR spectra of PMA-grafted PCN-222 and PMMA-grafted PCN-222 (Fig. S6) show good agreement for PMMA, while PMA is found to be slightly under-detected in Fig. 3. Strong C-H dipolar couplings in the MOF are observed (Fig. S7), which implies that detection of the CH peaks in multiCP (and DP) is reliable; this observation also indicates that there is on limited large-amplitude mobility of the MOF linkers.

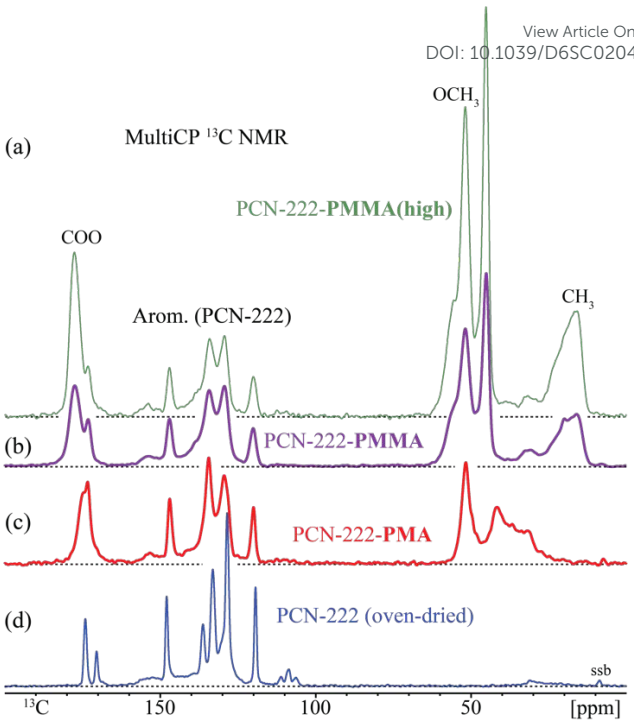

Fig. 3 Solid-state ^{13}C NMR spectra of polymer-grafted and neat PCN-222. (a) PCN-222 with excess PMMA. (b) PMMA-grafted PCN-222. (c) PMA-grafted PCN-222. (c) Neat oven-dried PCN-222.

NMR analysis of polymer–MOF proximity.

The spectra in Fig. 3 exhibit clear differences in the widths and positions of the peaks of the aromatic carbon atoms of the MOF linker, which indicates perturbations of the MOF linkers due to proximity to the polymer chains. This perturbation is strongest in the PMMA-grafted PCN-222. Such perturbations are also indicated by the shortening of the PCN-222 $T_{1\rho}$ relaxation times (Fig. S7). These can be due to changes in linker mobility or potentially because of transfer of magnetization from nearby polymer segments.

Two-dimensional ^{1}H-^{13}C heteronuclear correlation (HetCor) NMR with ^{1}H spin diffusion (see examples of spectra in Figs. S8-S11), provides even more direct evidence of proximity between most of the MOF linkers and some of the polymer. The time dependence of the cross peaks between the MOF and polymer in horizontal cross sections at the aromatic peak positions of the MOF (Figs. S8c-S11c) is shown in Fig. 4a and 4b for the PMA- and PMMA-grafted PCN-222, as well as PMMA-grafted UiO-66 for reference. The data show initial step increases, which can be attributed to polymer in close proximity to MOF linkers, while the slow rise at longer times is due to spin-diffusion between MOF and polymer on the ≥50-nm scale. This interpretation is bolstered by fit curves, see Fig. 4, from custom-designed simulations of spin diffusion between polymer and partially polymer-filled PCN-222 particles of a diameter of 140 nm and length of 380 nm based on SEM images.

View Article Online
DOI: 10.1039/D6SC03045G

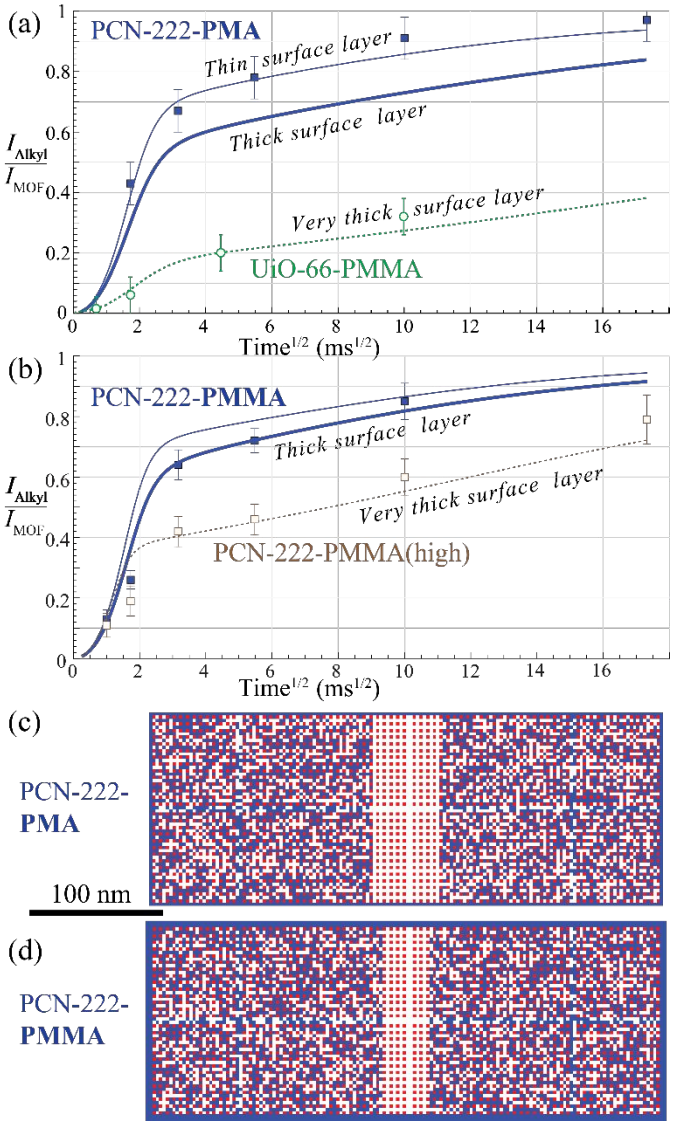

Fig. 4 Probing polymer-MOF proximity by ^{1}H-^{13}C HetCor NMR with ^{1}H spin diffusion, supported by detailed modelling. (a) ^{1}H spin diffusion from aromatic ^{1}H in PCN-222 to PMA (filled symbols and solid fit curves), normalized by the MOF-peak intensities.[27] Thick fit curves are for a thick, thin fit curve for a thin external polymer layer on the particle surface. For reference, data UiO-66-PMMA (open symbols and dashed curve), with little polymer intercalation and a thick polymer layer, are also included. (b) Same as (a) for PCN-222-PMMA. Open symbols and dashed curve: sample with a higher PMMA content and thicker external polymer layer. (c) Best-fit model of PMA-grafted PCN-222 in (a). (d) Best-fit model of PMMA-grafted PCN-222 producing the thick fit curve in (b) with MOF particle dimensions from SEM and relative amounts of polymer and MOF protons in the model based on NMR spectra. Polymer is blue, MOF linkers are red, and void pore space is white. The fast initial rise in the curves in (a) and (b) proves the polymer penetration into the MOF seen in both models (blue polymer inside the particles), while the height of the initial step constrains the thickness of the external blue polymer layer. The larger PMMA fraction results in a thicker external polymer layer. The central region of the MOF is kept polymer-free (no blue segments) because of limited polymer chain length.

More models, as well as simulations for PMMA- and PMA-grafted UiO-66, are included in Figs. S12-S14. When polymer is inside the pores and therefore in direct proximity to the MOF linkers, magnetization transfer is fast, within 10 ms. This fraction gives rise to the fast initial rise in the spin diffusion curves in Fig. 4; conversely, the height of this initial step is reduced by a thick external polymer layer as shown in Fig. 4d. The polymer:MOF ^{1}H ratio estimated from NMR spectra was an important parameter of these models. As shown in Fig. 4c and 4d, in the models the MOF particle was not only surrounded by a dense polymer layer, which is thicker with grafted PMMA than PMA, but also significantly filled with polymer, which accounts for the initial step in the spin diffusion curves and the observed effects of polymer on the MOF linker NMR spectrum and relaxation. The external PMMA layer is thicker presumably because the larger polymer amount exceeds the capacity of the MOF pores; for PCN-PMMA(high), this is clearly the case. UiO-66 with its smaller pores accommodates much less PMMA than PCN-222, see Fig. S14. The PMMA-grafted PCN-222 has a substantial external brush, see Fig. 4d, while the PMA-grafted MOF has a thinner external polymer layer, Fig. 4c. Therefore, in the SAMMs formation process requiring polymer entanglement, PCN-222-PMA fails to form a proper monolayer due to insufficient surface polymer brush. In contrast, PCN-222-PMMA with a relatively thicker external brush and UiO-66 with limited pore filling due to smaller pore size have sufficient surface polymer brush, resulting in successful SAMMs formation.

Conclusions

In conclusion, we demonstrate the first successful synthesis of polymer-grafted mesoporous PCN-222 nanorods using cat-CTA-anchored SI-PET-RAFT polymerization of PMA and PMMA, extending SAMMs beyond microporous UiO-66 systems. PMMA grafting yields free-standing SAMMs with tunable 1D-2D rod alignments through thick external brushes and mesopore infiltration, while flexible PMA causes aggregation and SAMMs failure due to thin surface coverage. Quantitative ^{13}C ssNMR reveals polymer-MOF ratios consistent with dual surface/partial pore filling by PMMA, evidenced by perturbed MOF linker peaks and accelerated $T_{1\rho}$ relaxation. ^{1}H-^{13}C HetCor with spin diffusion shows rapid initial cross-peaks from proximal polymer, with simulations confirming thicker PMMA brushes and pore filling alongside thinner PMA layers, explaining the assembly differences. This establishes polymer rigidity-pore interplay as a design principle for mesoporous hybrids. While the present study focuses on elucidating the structural mechanisms governing polymer-MOF interactions and SAMMs formation, the partial nature of pore filling confirmed by ssNMR suggests that residual porosity is retained, and future work optimizing polymer chain length and grafting density may enable functional films with tunable porosity for applications in catalysis and separations.

Author contributions

The manuscript was written through the contributions of all authors. M.K. and S.M.C. designed the materials and experimental strategy; M.K. conducted all experiments except ssNMR analysis; Z.S. and K.S.-R. performed ssNMR analysis; M.K. and K.S.-R. wrote the manuscript; S.M.C. supervised the editing of the manuscript. All authors have given approval to the final version of the manuscript.

Conflicts of interest

There are no conflicts to declare.

Data availability

The data supporting this article have been included as part of the Supplementary Information.

Acknowledgements

M.K. was supported by a grant from the National Science Foundation, Division of Materials Research under Award No. DMR-2205456; UCSD MRSEC, Award No. DMR-2011924). Additional support for materials and supplies were provided by the Department of Energy, Office of Basic Energy Sciences, Division of Materials Science and Engineering under award no. DE-FG02-08ER46519. SEM imaging was performed in part at the San Diego Nano-Technology Infrastructure (SDNI) of U.C. San Diego, a member of the National Nanotechnology Coordinated Infrastructure, which is supported by the National Science Foundation (ECCS-1542148). Funding for the solid-state NMR spectrometer utilized in this work was provided by the NSF MRI program (Award No. 1726346).

Notes and references

1. O. M. Yaghi, M. O'Keeffe, N. W. Ockwig, H. K. Chae, M. Eddaoudi and J. Kim, Reticular synthesis and the design of new materials, *Nature*, 2003, **423**, 705–714.
2. M. Eddaoudi, J. Kim, N. Rosi, D. Vodak, J. Wachter, M. O'Keeffe and O. M. Yaghi, Systematic Design of Pore Size and Functionality in Isoreticular MOFs and Their Application in Methane Storage, *Science*, 2002, **295**, 469–472.
3. N. Stock and S. Biswas, Synthesis of metal-organic frameworks (MOFs): routes to various MOF topologies, morphologies, and composites, *Chem. Rev.*, 2012, **112**, 933-969.
4. A. Schoedel, M. Li, D. Li, M. O'Keeffe and O. M. Yaghi, Structures of Metal-Organic Frameworks with Rod Secondary Building Units, *Chem. Rev.*, 2016, **116**, 12466-12535.
5. T. Kitao, Y. Zhang, S. Kitagawa, B. Wang and T. Uemura, Hybridization of MOFs and polymers, *Chem. Soc. Rev.*, 2017, **46**, 3108-3133.
6. L. E. Kreno, K. Leong, O. K. Farha, M. Allendorf, R. P. Van Duyne and J. T. Hupp, Metal-organic framework materials as chemical sensors, *Chem. Rev.*, 2012, **112**, 1105-1125.
7. X. Cui, K. Chen, H. Xing, Q. Yang, R. Krishna, Z. Bao, H. Wu, W. Zhou, X. Dong, Y. Han, B. Li, Q. Ren, M. J. Zaworotko and B. Chen, Pore chemistry and size control in hybrid porous materials for acetylene capture from ethylene, *Science*, 2016, **353**, 141-144.
8. M. Ding, X. Cai and H. L. Jiang, Improving MOF stability: approaches and applications, *Chem. Sci.*, 2019, **10**, 10209-10230.
9. M. Kalaj, K. C. Bentz, S. Ayala, Jr., J. M. Palomba, K. S. Barcus, Y. Katayama and S. M. Cohen, MOF-Polymer Hybrid Materials: From Simple Composites to Tailored Architectures, *Chem. Rev.*, 2020, **120**, 8267-8302.
10. K. Barcus and S. M. Cohen, Free-standing metal-organic framework (MOF) monolayers by self-assembly of polymer-grafted nanoparticles, *Chem. Sci.*, 2020, **11**, 8433-8437.
11. K. Barcus, P. A. Lin, Y. Zhou, G. Arya and S. M. Cohen, Influence of Polymer Characteristics on the Self-Assembly of Polymer-Grafted Metal-Organic Framework Particles, *ACS Nano*, 2022, **16**, 18168-18177.
12. M. Kang, P. A. Lin, J. A. Bunch, D. J. Lipomi, G. Arya and S. M. Cohen, Impact of Grafting Density on the Assembly and Mechanical Properties of Self-Assembled Metal-Organic Framework Monolayers, *J. Am. Chem. Soc.*, 2025, **147**, 6966-6973.
13. J. Xiao, Z. Shi, M. Cong, D. Wang, H. Qin, Q. Li, W. Lu, Z. Guo, X. Liang and G. Qing, Photoswitchable Nanoporous Metal–Organic Framework Monolayer Film for Light-Gated Ion Nanochannel, *ACS Applied Nano Materials*, 2023, **6**, 2813-2821.
14. J. H. Cavka, S. Jakobsen, U. Olsbye, N. Guillou, C. Lamberti, S. Bordiga and K. P. Lillerud, A New Zirconium Inorganic Building Brick Forming Metal Organic Frameworks with Exceptional Stability, *J. Am. Chem. Soc.*, 2008, **130**, 13850-13851.
15. D. Feng, Z. Y. Gu, J. R. Li, H. L. Jiang, Z. Wei and H. C. Zhou, Zirconium-metalloporphyrin PCN-222: mesoporous metal-organic frameworks with ultrahigh stability as biomimetic catalysts, *Angew. Chem. Int. Ed.*, 2012, **51**, 10307-10310.
16. Y. He, C. Li, X. B. Chen, Z. Shi and S. Feng, Visible-Light-Responsive UiO-66(Zr) with Defects Efficiently Promoting Photocatalytic CO(2) Reduction, *ACS Appl. Mater. Interfaces*, 2022, **14**, 28977-28984.
17. Z. Wei, S. Song, H. Gu, Y. Li, Q. Sun, N. Ding, H. Tang, L. Zheng, S. Liu, Z. Li, W. Chen, S. Li and S. Pang, Enhancing the Photocatalytic Activity of Zirconium-Based Metal-Organic Frameworks Through the Formation of Mixed-Valence Centers, *Adv. Sci.*, 2023, **10**, e2303206.
18. M. Sarker, S. Shin, J. Jeong and S. Jhung, Mesoporous metal-organic framework PCN-222(Fe): Promising adsorbent for removal of big anionic and cationic dyes from water, *Chem. Eng. J.*, 2019, **371**, 252-259.
19. B. L. Bonnett, E. D. Smith, M. De La Garza, M. Cai, J. V. t. Haag, J. M. Serrano, H. D. Cornell, B. Gibbons, S. M. Martin and A. J. Morris, PCN-222 Metal-Organic Framework Nanoparticles with Tunable Pore Size for Nanocomposite Reverse Osmosis Membranes, *ACS Appl Mater Interfaces*, 2020, **12**, 15765-15773.
20. M. Kang and S. M. Cohen, Synthesis and Characterization of Self-Assembled Metal-Organic Framework Monolayers using Polymer-coated Particles, *J. Vis. Exp.*, 2024, DOI: 10.3791/66497, e66497.
21. J. Chiefari, Y. K. Chong, F. Ercole, J. Krstina, J. Jeffery, T. P. T. Le, R. T. A. Mayadunne, G. F. Meijs, C. L. Moad, G. Moad, E. Rizzardo and S. H. Thang, Living Free-Radical Polymerization by Reversible Addition-Fragmentation Chain Transfer: The RAFT Process, *Macromolecules*, 1998, **31**, 5559-5562.
22. R. Yin, H. Wu, X. Hu, K. Kim, F. Lorandi, D. R. D'hooge, E. M. Benetti, M. R. Bockstaller and K. Matyjaszewski, Effect of Initiator Density, Catalyst Concentration, and Surface Curvature on the Uniformity of Polymers Grafted from Spherical Nanoparticles, *Macromolecules*, 2026, **59**, 689-701.

View Article Online
DOI: 10.1039/D6SC02045C

23. Y. Reyes, G. Arzamendi, J. M. Asua and J. R. Leiza, Branching at High Frequency Pulsed Laser Polymerizations of Acrylate Monomers, *Macromolecules*, 2011, **44**, 3674-3679.
24. T. Junkers and C. Barner-Kowollik, The role of mid-chain radicals in acrylate free radical polymerization: Branching and scission, *J. Polym. Sci. A Polym. Chem.*, 2008, **46**, 7585-7605.
25. B. Metin and F. D. Blum, Molecular mass and dynamics of poly(methyl acrylate) in the glass-transition region, *J. Chem. Phys.*, 2006, **124**, 054908.
26. R. P. Kusy, W. F. Simmons and A. R. Greenberg, Glass transition temperature of poly(methyl methacrylate) blends *Polymer*, 1981, **22**, 268-270.
27. Z. Sun, S. Yuan and K. Schmidt-Rohr, Quantification of Large Long Periods in Rigid Polymer Systems by 1H Spin Diffusion in HetCor NMR with Heavy Peak Overlap, *Appl. Magn. Reson.*, 2023, **54**, 1135-1163.

View Article Online
DOI: 10.1039/D6SC02045C

The data supporting this article have been included as part of the Supplementary Information.